Quaternary International 211 (2010) 4–13

Contents lists available at ScienceDirect

Quaternary International

journal homepage: www.elsevier.com/locate/quaint

Morphological and morphometric analysis of variation in the Zhoukoudian *Homo erectus* brain endocasts

Xiujie Wu [a,b,*], Lynne A. Schepartz [c], Christopher J. Norton [d]

[a] *Laboratory of Evolutionary Systematics of Vertebrates, Institute of Vertebrate Paleontology and Paleoanthropology, Chinese Academy of Sciences, Xizhimenwaidajie 142, Box 643, Beijing 100044, China*
[b] *State Key Laboratory of Palaeobiology and Stratigraphy, Nanjing Institute of Geology and Palaeontology, Nanjing 210008, China*
[c] *Department of Anthropology, Florida State University, Tallahassee, FL 32306-7772, USA*
[d] *Department of Anthropology, University of Hawaii at Manoa, Honolulu, HI 96822-2223, USA*

ARTICLE INFO

Article history:
Available online 19 July 2009

ABSTRACT

The six Zhoukoudian (ZKD) Locality 1 *Homo erectus* specimens derive from stratigraphic levels 11–3 with a geochronological span of approximately 0.3 Ma. This paper introduces the history of the ZKD endocasts and presents data on their morphological features and linear dimensions in order to evaluate variability in the sample over time and in the broader context of human brain evolution using a comparative sample of African and other Asian *H. erectus* fossils and modern Chinese males. The ZKD brains are very similar in their morphological characteristics, but there are also significant but subtle changes involving expansion of the frontal and occipital lobe breadths that correlate with the geochronology. The same is not true for general endocranial volume. The ZKD brains, together with other Asian and African *H. erectus* specimens, have low height dimensions and short parietal chords that distinguish them from the modern Chinese. Furthermore, the lack of geographical patterning in the fossil sample, as determined by Principal Components Analysis, provides no support for arguments advocating the splitting of *H. erectus* into separate taxa.

1. Introduction

The endocast is the impression taken from the inside of a cranium that retains the surface features of the brain. It does not display the original brain anatomy, but instead reflects the external features of brain anatomy in detail. Studying endocasts of fossil hominins allows researchers to make inferences on functional anatomy, physiology, and phylogeny (Bruner, 2003). Thus, endocasts from fossil crania are unquestionably the most important materials for analyzing and understanding human brain evolution (Holloway, 1980; Falk, 1985; Begun and Walker, 1993; Broadfield et al., 2001; Bruner, 2004). Because hominin fossils are very rare, and their crania are often fragmentary, distorted, or not sufficiently prepared for endocasting, the number of hominin endocasts available for analysis is quite limited and few are complete enough for morphometric comparisons. The Chinese Zhoukoudian (ZKD) *Homo erectus* endocasts, a group of six specimens from a single locality, provide fundamental data for studying hominin brain evolution.

For more than 70 years, a number of scholars conducted research on the ZKD endocasts (e.g., Black, 1932, 1933; Dubois, 1933; Ariens-Kappers, 1934; Shellshear and Smith, 1934; Weidenreich, 1936; Ariens-Kappers and Bouman, 1939; Broadfield et al., 2001; Holloway et al., 2004; Wu et al., 2009). These investigations began in 1931 when Davidson Black manually reconstructed the endocast of ZKD skull III (Locus E) using plaster. He suggested the brain was essentially human in its form, that the individual was right handed, and that there was evidence for the neurological underpinnings of articulate speech (Black, 1932, 1933). His work initiated the study of the actual brains of ancient humans and apes. Shellshear and Smith (1934) argued that ZKD III displayed primitive characters that did not appear in *Pithecanthropus erectus* such as a flat frontal lobe and a well-marked frontal keel. In the summer of 1930, a number of skull fragments from Locus D were refitted as the adult ZKD II. Weidenreich (1935) reconstructed the ZKD II endocast. Subsequently in 1936, ZKD X (Skull I of Locus L), ZKD XI (Skull II of Locus L) and ZKD XII (Skull III of Locus L) were found. These three endocasts were reconstructed by Weidenreich (1938, 1941). The endocast of ZKD V was reconstructed in 1973

* Corresponding author. Laboratory of Evolutionary Systematics of Vertebrates, Institute of Vertebrate Paleontology and Paleoanthropology, Chinese Academy of Sciences, Xizhimenwaidajie 142, Box 643, Beijing 100044, China. Tel.: +86 10 88369124; fax: +86 10 68337001.
E-mail address: wuxiujie@ivpp.ac.cn (X. Wu).

1040-6182/$ – see front matter © 2009 Elsevier Ltd and INQUA. All rights reserved.
doi:10.1016/j.quaint.2009.07.002

based on five fragments of cranium found in Locus H III. Two fragments, consisting of the temporal and adjoining parietal and occipital bones, were excavated in 1934 and described by Weidenreich (1935). More fragments of the cranium, including the frontal, parietal, sphenoid and occipital bones, were found in 1966. The endocranial volume was determined (Qiu et al., 1973), but no detailed analysis of the endocast was undertaken until recently (Wu et al., 2009).

In addition to the works on the ZKD endocasts mentioned above, some broader comparative studies have included the ZKD specimens. For example, Begun and Walker (1993) compared the endocast of KNM-WT 15000 with ZKD II, III, X and XII. They found that the overall morphology of those specimens was quite similar to KNM-WT 15000. However, they also found that the four ZKD endocasts can be distinguished from KNM-WT 15000 by the development of the superior sagittal sinus and the apparently well-developed connection between the sphenoparietal sinus and the middle meningeal veins. Broadfield et al. (2001) found that the endocast of Sambungmacan (Sm) 3 has a mosaic of features that are shared with both other Indonesian *H. erectus* and ZKD III. Wu et al. (2006) compared the endocast of Hexian with ZKD (II, III, X, XI and XII), Sm 3 and KNM-WT 15000, and determined that Hexian is most similar to the ZKD *H. erectus* specimens.

The ZKD hominins included in this study all derive from the principal locality at Zhoukoudian designated Locality 1; a cave complex located 50 km southwest of Beijing, China. The stratigraphic sequence was extensively studied and its designations were revised by the different excavators, most notably Teilhard de Chardin, Davidson Black and Jia Lanpo. ZKD III was found in Black's Layer 11 (Pei, 1929; Black et al., 1933; Lin, 2004) or Jia's Layer 10 (Jia, 1959). ZKD X, XI and XII are from Layer 8/9 (Black et al., 1933; Jia, 1959). ZKD II is from Black's Layer 8/9 or Jia's Layer 10. ZKD V was found in Layer 3 (Jia, 1959). Fig. 1 illustrates the approximate spatial relationships of the six crania we used in this paper. ZKD V was found in Layer 3; ZKD II, X, XI and XII are from Layer 8/9, and ZKD III was found in Layer 11 (Lin, 2004).

A series of different dating studies have been conducted to determine the absolute ages of the ZKD strata. Electron spin resonance (ESR) dating of mammal teeth collected from Layers 3, 4, 6–9, 11 and 12 suggests an age range of 0.28–0.58 Ma for the fossils (Huang et al., 1993; Grün et al., 1997) with ZKD III at 0.58 Ma, ZKD II, X, XI and XII all at approximately 0.42 Ma. The stratigraphically highest specimen is ZKD V at 0.28 Ma. However, thermal ionization mass spectrometric (TIMS) $^{230}Th/^{234}U$ dating on intercalated speleothem samples suggests that the age of the ZKD fossils is between 0.4 and 0.8 Ma (Shen et al., 2001). As a result, the age of ZKD V is >0.4 Ma, possibly in the range of 0.4–0.5 Ma. The age of the hominin fossils from the lower strata is at least 0.6 Ma, and possibly 0.8 Ma or older (Shen et al., 2001). Shen et al.'s (2009) new dating study, based upon cosmogenic $^{26}Al/^{10}Be$ burial dating on quartz grains, suggests that the ages of Layers 7–10 of ZKD are between 0.68 and 0.78 Ma (Shen et al., 2009). The new age estimates imply that the early ZKD specimens are probably contemporaneous with Sangiran 17 that may date to 0.7 Ma (Swisher et al., 1994). While the dating of the ZKD Locality I deposits is still debated, all of the results document a considerable span of time (as much as 0.3–0.5 Ma) between the oldest and youngest hominin fossils. An appreciation of this temporal diversity is critical for any understanding of ZKD hominin morphological variability.

This paper describes and interprets the morphology of the six ZKD brain endocasts and compares them with endocasts from China (Hexian, modern Chinese), Indonesia (Trinil II, Sangiran 2, 10, 12, 17, Sm 3) and Africa (KNM-ER 3733, 3883, KNM-WT 15000 and Salé) to develop a broader picture of variation at ZKD and in *H. erectus* generally.

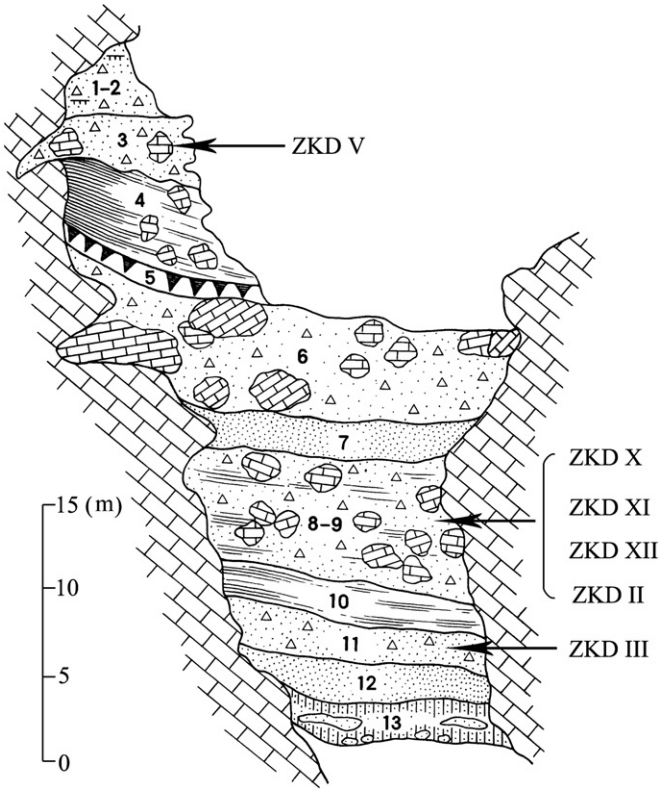

Fig. 1. Composite section of West Profile, ZKD Locality 1 showing the stratigraphic positions of the cranial discoveries (Adapted from Jia, 1959).

2. Materials and methods

2.1. Endocasts

Table 1 is the catalogue of endocasts used in this study. The specimens include representatives of Asian *H. erectus* (ZKD, Hexian, Trinil II, Sangiran 2, 10, 12, 17, and Sm 3) and an outgroup of African presapiens populations (KNM-ER 3733, 3883, KNM-WT 15000 and Salé). Endocasts of ZKD III, ZKD II, ZKD X, ZKD XI, ZKD XII, ZKD V, Hexian and Trinil II are from the collections of the Institute of Vertebrate Paleontology and Paleoanthropology, Chinese Academy of Sciences. The six ZKD endocasts are excellent first-generation casts prepared from the original fossils. They therefore preserve more detailed information than can be observed on the later generation casts that are available to most researchers conducting comparative endocast studies. Endocasts of 31 modern Chinese males were made by the first author (Wu et al., 2006). They provide a dataset representing general aspects of modern human brain variation. Data for the endocasts of Sm 3, Sangiran 2, 10, 12, Sangiran 17, KNM-ER 3733, 3883, KNM-WT 15000 and Salé are from published studies (see Table 1). The cranial capacities of all endocasts in the study are obtained by water displacement.

2.2. Methods

The research methodology employed here includes visual inspection, descriptions of gross brain morphology, and then quantification of size and shape differences.

Fig. 2 illustrates the principal regions of an endocast: the frontal lobe, parietal lobes, temporal lobes, occipital lobe and the cerebellum. The specific features compared here are also indicated

Table 1
Age (Ma) and cranial capacity (ml) for endocasts used in the study.

Endocast	Date (Ma)	Cranial capacity (ml)	Literature
ZKD III (Skull III, Locus E, Layer 11)	>0.80	915	Black et al., 1933; Weidenreich, 1943; Shen et al., 2001
ZKD II (Skull II, Locus D I, Layers 8–9)	0.68–0.78	1020	Black et al., 1933; Weidenreich, 1943; Shen et al., 2009
ZKD X (Skull X, Locus L I, Layers 8–9)	0.68–0.78	1225	Black et al., 1933; Weidenreich, 1943; Shen et al., 2009
ZKD XI (Skull XI, Locus L II, Layers 8–9)	0.68–0.78	1015	Black et al., 1933; Weidenreich, 1943; Shen et al., 2009
ZKD XII (Skull XII, Locus L III, Layers 8–9)	0.68–0.78	1030	Black et al., 1933; Weidenreich, 1943; Shen et al., 2009
ZKD V (Skull V, Locus H III, Layer 3)	>0.40	1140	Weidenreich, 1943; Qiu et al., 1973; Shen et al., 2001
Hexian	0.41	1025	Wu and Dong, 1982; Grün et al., 1998
Trinil II	<1.0	940	Holloway, 1981; Swisher et al., 1994
Sm 3	0.9	917	Broadfield et al., 2001; Delson et al., 2001
Sangiran 2	0.98	813	Holloway, 1981; Swisher et al., 1994
Sangiran 10	1.2	855	Holloway, 1981; Swisher et al., 1994
Sangiran 12	0.9	1059	Holloway, 1981; Swisher et al., 1994
Sangiran 17	0.7	1004	Holloway, 1981; Swisher et al., 1994
KNM-ER 3733	1.75	848	Holloway, 1981; Brown et al., 1985
KNM-ER 3883	1.57	804	Holloway, 1981; Brown et al., 1985
KNM-WT 15000	1.51	880	Begun and Walker, 1993; Brown and McDougall, 1993
Salé	0.40	880	Holloway, 1981; Brown et al., 1985
Modern Chinese ($n = 31$)	Recent	1110–1600	This study

(Fig. 2A–D): the lateral Sylvian fissure area, middle meningeal artery, sagittal keel (the prominence along the midline or sagittal plane of the parietal or frontal lobes), venous sinuses, frontal pole, occipital pole, Broca's cap (the posterior surface of the third frontal circumvolution) and frontal keel (a well-marked and prominent orbital margin). The method for determining frontal and occipital petalial patterns of asymmetry derives from LeMay et al. (1982), who score which hemisphere protrudes further rostrally for the frontal petalia and caudally for the occipital petalia, in addition to which hemispheres are the broadest.

Following Begun and Walker (1993), nine linear measures were taken to provide quantification of the overall shape of the endocasts (Table 2). The landmarks and standardized measurements are described in detail by Wu et al. (2006). To take the measurements, the endocast rests with the axis of the frontal and occipital poles parallel to the table surface when viewed superiorly or laterally. The length is measured from the anterior-most position of the frontal lobe to the greatest posterior protrusion of the occipital lobe. The breadth is the maximum width of the greatest lateral protrusion of the endocast. The height is a projection from the highest point on the parietal lobe to the most inferior point of the right cerebellar hemisphere. Frontal breadth is the dimension between the greatest lateral protrusions of the frontal lobe. Cerebral height is from the highest point of the parietal lobe to the most inferior point of the right temporal lobe. The frontal height is a projection from bregma to the most ventral point of the right frontal lobe. The frontal chord is bregma to the most anterior protuberance of the right frontal lobe. The parietal chord is from bregma to lambda. The occipital

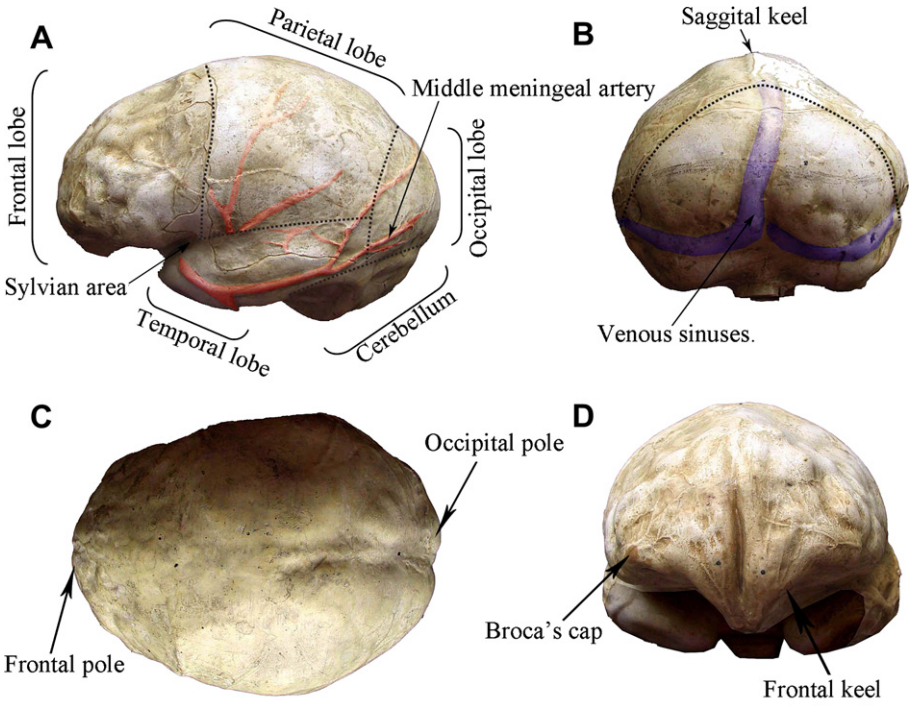

Fig. 2. Lateral view (A), posterior view (B), superior view (C) and anterior view (D) of an endocast, indicating anatomical landmarks. The lobes are delineated by dotted lines.

Table 2
Endocast measurements (mm).

	Length	Breadth	Height	Frontal breadth	Cerebral height	Frontal height	Frontal chord	Parietal chord	Occipital breadth
ZKD III	156.1	120.4	99.7	91.9	98.9	73.1	78.2	86.9	87.3
ZKD II	161.1	116.2	106.4	94.2	107.2	78.2	75.9	94.5	89.9
ZKD X	174.2	128.7	114.8	106.7	116.2	88.2	85.3	95.9	95.5
ZKD XI	166.1	127.2	103.7	97.1	105.4	79.0	70.2	87.2	93.3
ZKD XII	167.6	127.8	108.5	97.8	107.3	79.9	82.6	87.5	95.0
ZKD V	174.9	128.0	108.2	110.1	108.9	74.8	82.0	87.1	99.1
Hexian	159.4	134.8	100.7	99.8	102.0	75.9	69.1	92.2	96.6
Trinil II	156.1	125.4	97.9	94.3	102.1	77.9	75.6	83.0	92.2
Sm 3	154.0	121.0	103.0	107.0	99.0	68.0	73.0	83.0	91.0
Sangiran 2	148.0	120.0	89.8	93.7	93.0	70.3	68.4	70.0	92.0
Sangiran 10	154.5	115.2	92.5	85.6	95.6	66.9	77.5	80.9	97.7
Sangiran 12	159.1	127.1	97.0	93.9	98.3	66.5	73.5	92.0	103.0
Sangiran 17	161.0	131.0	97.5	108.5	97.0	72.0	73.9	93.0	101.0
KNM-ER 3733	146.0	122.0	98.5	102.2	97.0	73.1	71.9	97.0	95.0
KNM-ER 3883	150.1	118.8	89.9	84.9	97.2	72.2	70.2	82.7	106.7
KNM-WT 15000	158.0	116.0	100.0	86.0	107.0	66.0	73.0	93.0	103.0
Salé	155.9	120.5	91.2	92.9	95.1	68.4	68.6	89.9	90.1
Modern humans ($n = 31$)	159.8–177.0	117.0–137.3	119.8–135.2	102.9–122.3	110.9–133.8	86.1–99.9	69.2–89.0	97.9–114.1	91.5–107.5

breadth is maximum width of the occipital lobe perpendicular to the sagittal plane.

Statistical analyses were performed using SPSS 13.0. Bivariate plots and a non-parametric statistic the Wilcoxon Signed Ranks test were used to evaluate whether the dimensions of the ZKD specimens are significantly different. Tests of association (Spearman rank-order correlations) between the measures of the ZKD specimens were performed to identify the bivariate dimensions with significant correlations at the 0.01 level.

Principal component analyses (PCA) provide a perspective on metric variation among the endocasts of ZKD and other specimens. In order to run the PCA, the variables were scaled and the values standardized. PCA included two components: 1) one with 48 specimens (17 fossils and 31 moderns) and nine log-transformed measurements [log(length), log(breadth), log(height), log(frontal breadth), log(cerebral height), log(frontal height), log(frontal chord), log(parietal chord), and log(occipital breadth)]; 2) and another with the same 48 specimens and 8 ratio measurements (breadth/length, height/length, height/breadth, occipital breadth/frontal breadth, frontal chord/parietal chord, frontal breadth/breadth, occipital breadth/breadth and frontal height/cerebral height).

3. Results

3.1. Gross morphology of the ZKD endocasts

Fig. 3 provides six views of the five ZKD endocasts arranged in chronological order to facilitate comparisons. The inferior view with the cranial base is not included as the majority of the basicranium is missing due to taphonomic, primarily postdepositional, damage to all of the crania.

ZKD III (Locus E – 1932). The endocast is mostly complete except for the base or foramen magnum area, the whole basi-occipital, and the ethmoid region together with most of the sphenoid (Fig. 3, A1–A5). It is widest at the level of the parietal eminences that are situated one-third of the way from the occipital poles. Viewed superiorly (Fig. 3, A1), the cast is long and narrow. From the parietal eminence the brain surface slopes downward in all directions. Sagittal keeling occurs along the central axis of the parietal lobe. Viewed anteriorly (Fig. 3, A2), the frontal region of the endocast is flattened bilaterally and bulges in the center of the frontal lobe. The frontal cap forms a salient landmark in front of the most anterior point of the temporal pole. In front of the frontal cap, the orbital margin is full and passes forward to end in a well-marked and prominent frontal keel. The left insular operculum of the frontal area is remarkably developed in size and prominence relative to its counterpart on the right. Viewed laterally (Fig. 3, A3–A4), the parietal region of this endocast is most prominent and the frontal region is flattened. The lower border of the frontal lobe and the upper border of the temporal pole are beveled. The temporal region is narrow and the temporal pole is long and slender. The middle meningeal vessels, visible in this view, are divided into three branches on both the left and right. Upon entering the middle cranial fossa, the middle meningeal vessels divide into a short anterior branch that courses toward the temporal pole, and a much longer posterior branch that caudally and becomes elaborated in the region of the occipital parietal cortex. In posterior view (Fig. 3, A5) the occipital forms a triangular elevation on the posterior aspect of the cast. The occipital lobe is dorso-ventrally flattened and has strong posterior projection, and the occipital poles are especially prominent and rounded. The superior sagittal sinus is divided into two branches and deviates to the right. ZKD III manifests R-frontal and R-occipital petalial width patterns.

ZKD II (Locus D – 1935). The endocast of ZKD II consists of part of the frontal lobe, the two parietal lobes, the greater part of the left temporal lobe, and three small fragments of the occipital lobe (Fig. 3, B1–B5). The widest point is situated at the lateral border of the temporal lobes. Viewed superiorly (Fig. 3, B1), the cast is long and very narrow. From the parietal eminence the brain slopes downward in all directions. Sagittal keeling is also characteristic of this specimen. Viewed anteriorly (Fig. 3, B2), the frontal region is flattened. The orbital margin of the left frontal lobe is full. In lateral view (Fig. 3, B3–B4), the left temporal region is narrow and the temporal pole is long and slender. The middle meningeal vessels are shown on the right side. They have a much longer posterior branch that courses caudally and becomes elaborated in the region of the occipital parietal cortex.

ZKD X (Locus L I – 1938). The endocast of ZKD X is almost complete, and includes almost the entire frontal lobe except for the lateral portion of the left side; the two parietal lobes, the entire occipital lobe, nearly the entire right temporal lobe, and two small fragments of the left temporal lobe (Fig. 3, C1–C5). The entire base and the pterion region on both sides are missing. It is widest at the level of the lateral border of the temporal lobes, approximately one-third of the length from the occipital lobe. Viewed superiorly (Fig. 3, C1), the endocast is long and narrow. From the prominent vertex the brain slopes downward in all directions. Sagittal keeling occurs along the central axis of the parietal lobes. Viewed anteriorly

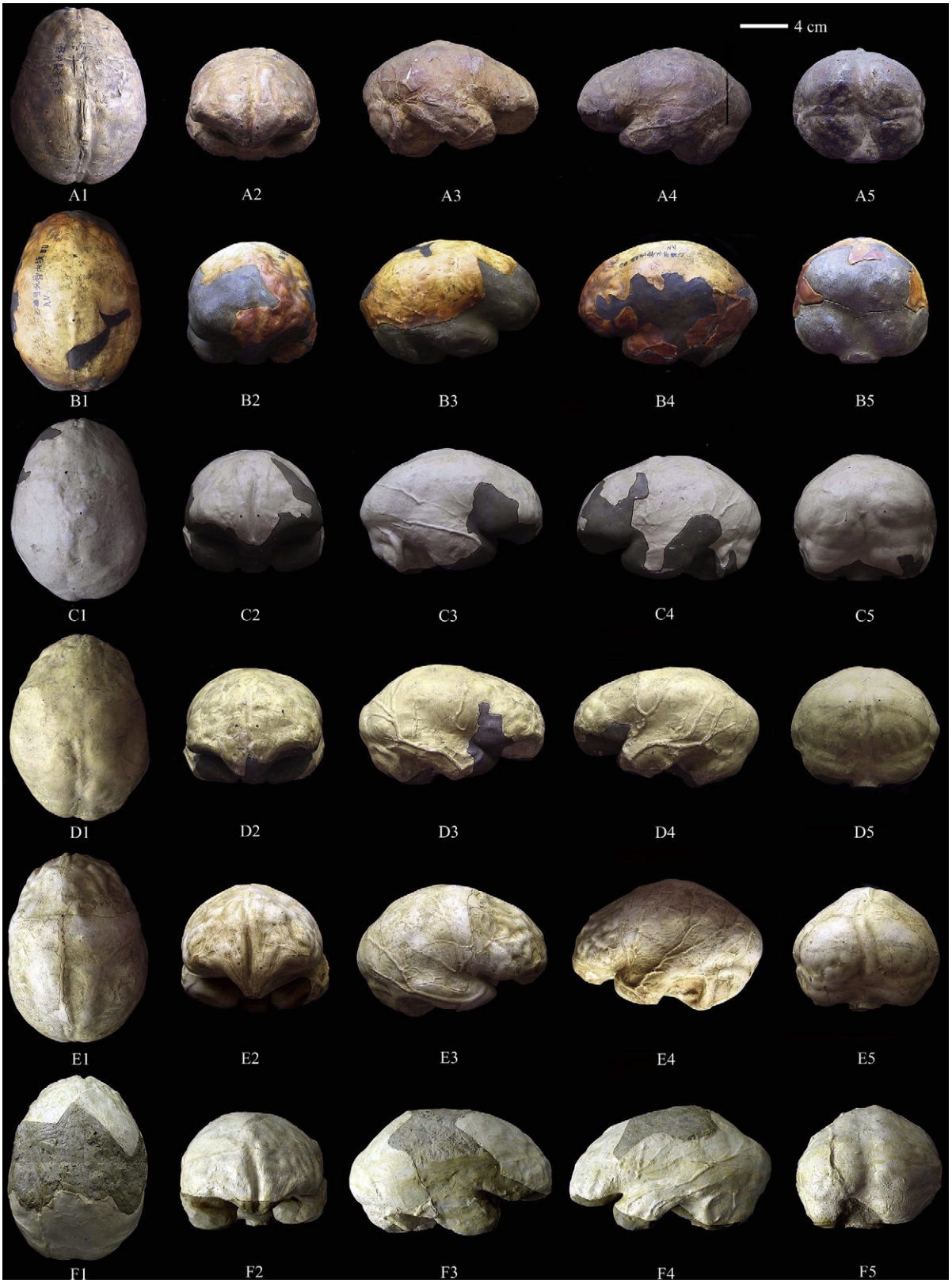

Fig. 3. From left to right: superior, frontal, right lateral, left lateral and posterior views of the six ZKD endocasts. They are in chronological order with the geologically youngest, ZKD V, in the bottom row. A1–A5: ZKD III; B1–B5: ZKD II; C1–C5: ZKD X; D1–D5: ZKD XI; E1–E5: ZKD XII; F1–F5: ZKD V.

(Fig. 3, C2), the frontal region bulges on both sides. As the pterion region is missing, the form of the frontal cap and frontal keel cannot be determined. As for the frontal, the temporal region is also prominent and bulging. Meningeal vessels are visible on both sides. On the right, the posterior ramus divides into two branches (Fig. 3, C3). The anterior ramus is smaller than the posterior and has a very small and short branch along the fissure of Sylvain area. On the left side (Fig. 3, C4), the posterior ramus has more branches than the anterior ramus. In posterior view (Fig. 3, C5) the occipital has a semi-ovoid shape. There is asymmetry of the occipital poles, with the left pole positioned more posteriorly than the right. The superior and inferior polar eminences are asymmetrical bilaterally. The position of the superior and inferior polar eminences on the right are higher than on the left, but the superior and inferior polar eminences on the left are posterior to those of the right side. The groove for the superior sagittal sinus is visible from lambda. The sagittal sinus runs downward along the groove and its course deviates somewhat to the right. ZKD X shows L-frontal and R-occipital petalial width patterns.

ZKD XI (Locus L II – 1938). The endocast of ZKD XI includes the frontal lobes, the parietal lobes, the occipital lobe, and the temporal lobes (Fig. 3, D1–D5). The basal portions anterior to the foramen magnum are missing. The endocast is widest at the level of the lateral border of the temporal lobes, at one-third of the length from the occipital lobe. Viewed superiorly (Fig. 3, D1), the endocast is long and narrow. From the highest point located centrally on the parietal lobes, the brain slopes downward in all directions. There are bilateral depressions of the parietal lobes. Sagittal keeling is characteristic of this specimen. Viewed anteriorly (Fig. 3, D2), the frontal region is flattened. The frontal cap forms a salient landmark in front of the most anterior point of the temporal pole. Viewed laterally (Fig. 3, D3–D4), the Sylvian area shows a distinct depression at the lower anterior region of the parietal lobe extending to the upper region of the temporal lobe. The temporal region is narrow and the temporal pole is long and slender. The meningeal vessels are well preserved on both sides. The posterior rami are well developed and have finer branches than the anterior rami. In posterior view (Fig. 3, D5) the occipital forms a triangular elevation on the posterior aspect of the cast. The positions of the superior and inferior polar eminences on the right are higher and more posterior than the left ones. The superior sagittal sinus is visible beginning as a narrow ridge between the rostral cerebral poles, and becomes marked at bregma. At the confluence, the superior sagittal sinus becomes continuous with the right transverse sinus. ZKD XI shows L-frontal and L-occipital petalial width patterns.

ZKD XII (Locus L III – 1938). The frontal lobe of the endocast of ZKD XI is preserved almost completely, along with the left temporal lobe, the entire occipital lobe including the posterior margin of the occipital foramen, and nearly the entire right temporal lobe (Fig. 3, E1–E5). ZKD XII is practically identical to ZKD XI, sharing all of the features described above. ZKD XII shows L-frontal and L-occipital petalial width patterns.

ZKD V (Locus H III – 1973; highest in the stratigraphic sequence). The frontal and occipital lobes of ZKD V are almost complete, but the base and part of the parietal lobes are missing (Fig. 3, F1–F5). Viewed superiorly (Fig. 3, F1), the endocast is long and narrow. Viewed anteriorly (Fig. 3, F2), the frontal region of the cast is flattened bilaterally and bulges in the center of the frontal lobe. The frontal cap forms a salient landmark in front of the most anterior point of the temporal pole. The orbital margin is full and ends in a well defined and prominent frontal keel. Viewed laterally (Fig. 3, F3–F4), the temporal lobes are narrow, and the Sylvian area between the temporal and frontal lobes is a distinct depression. The middle meningeal vessels are visible on the left side, and the pattern is identical to that observed on ZKD XI and ZKD XII. According to the preserved part on the left, the parietal lobes are filled-out and bossed (Fig. 3, F4). The occipital lobe is dorso-ventrally flattened with strong posterior projection, and the occipital poles are especially prominent and rounded. The cerebellar lobes are anterior to the occipital lobe. Viewed posteriorly (Fig. 3, F5), the superior longitudinal sinus groove becomes continuous with the right sagittal sinus. ZKD V shows L-frontal and R-occipital petalial width patterns.

As the above descriptions illustrate, the overall morphological similarities among the ZKD endocasts are striking and notable. This corresponds with the observations of Weidenreich (1943), who emphasized the shared characteristics of the crania.

3.2. Comparison with other endocasts

The following observations are provided to highlight the differences between the ZKD endocasts and the comparative materials. In general, the widest point or greatest breadth of most modern Chinese endocasts in this sample is situated at midway along the length of the cast. In the ZKD endocasts and the other *H. erectus* specimens, the widest point is usually located lower and more posteriorly.

The surfaces of the frontal lobe of the *H. erectus* specimens (with the exception of Sm 3) are flat, whereas the frontal lobes of the modern Chinese are full and rounded. The frontal keel is prominent on the ZKD specimens, Hexian, Trinil II, Sangiran 2, Sangiran 10, Sangiran 12 and Sangiran 17, but is not present on Sm 3, KNM-ER 3733, KNM-ER 3883, Salé, KNM-WT 15000 and the modern Chinese specimens. The area of the inferior frontal gyrus is slightly larger and more prominent on the left side in all of the fossil endocasts and the modern Chinese specimens compared here.

The ZKD III, II, X, XI, XII, and Hexian endocasts have sagittal keels and depressed Sylvian areas (seen only on the left for Hexian and ZKD V), in contrast to the flat, undepressed regions that characterize other *H. erectus* endocasts. Some of the modern Chinese in our sample have a weak sagittal keel but they lack depressed Sylvian areas. Superiorly, the parietal lobes of the ZKD specimens and Hexian are depressed, while other comparative endocasts have round and full parietal lobes.

The temporal lobes of the ZKD endocasts are narrow and slender. In contrast, Hexian, Sm 3, Trinil II, Sangiran 2, Sangiran 12, Sangiran 17, KNM-ER 3733, KNM-ER 3883, KNM-WT 15000 and the modern Chinese have fuller and broader temporal lobes.

The occipital lobes of the ZKD specimens, Hexian, Sangiran 2, Sangiran 10, Sangiran 12, Sangiran 17 and Salé are dorso-ventrally flattened and have strong posterior projections; the occipital lobes of Sm 3, Trinil II, KNM-ER 3733, KNM-ER 3883, KNM-WT 15000 and the modern Chinese are round and lack strong posterior projections. The cerebellar lobes are low and anterior to the occipital lobes for the ZKD and other hominin endocasts in our sample. In the modern Chinese sample, the cerebellar structures are more globular, posteriorly positioned, and compact in their overall form.

The meningeal vessels of ZKD, Hexian, Sangiran 2, Sangiran 10, Sangiran 12, Sangiran 17, Trinil II, and Sm 3 are similar as they all have more branches overlying the middle to posterior regions (see also Begun and Walker, 1993; Grimaud-Hervé, 1997; Holloway et al., 2004). The anterior branch of the middle meningeal system appears to be more developed on Salé, KNM-WT 15000, and the modern Chinese in the sample. The venous sinus pattern varies among the specimens, and there are no distinct patterns that clearly distinguish the fossils from the modern comparative materials. The petalia patterns of the ZKD endocasts are variable, which is not the pattern characteristic of most modern humans (cf. Holloway and De La Coste-Lareyondie, 1982).

Table 3
Spearman rank-order correlations among the nine dimensions of the ZKD specimens.

	Length	Breadth	Height	Frontal breadth	Cerebral height	Frontal height	Frontal chord	Parietal chord	Occipital breadth
Length	1.000	.886*	.771	1.000**	.886*	.429	.600	.257	1.000**
Breadth		1.000	.771	.886*	.829*	.543	.771	.257	.886*
Height			1.000	.771	.943**	.771	.829*	.714	.771
Frontal breadth				1.000	.886*	.429	.600	.257	1.000**
Cerebral height					1.000	.600	.771	.600	.886*
Frontal height						1.000	.486	.829*	.429
Frontal chord							1.000	.371	.600
Parietal chord								1.000	.257
Occipital breadth									1.000

**Significant at the 0.01 level (2-tailed). *Significant at the 0.05 level (2-tailed).

3.3. Metrical comparisons

3.3.1. Endocranial volume and metric data

Cranial capacities and geologic ages for the endocasts used in the study are listed in Table 1. The cranial capacity of the oldest ZKD *H. erectus* (ZKD III) is 915 ml; the average volume of ZKD II, ZKD X, ZKD XI, and ZKD XII is 1072 ml; and the youngest ZKD *H. erectus* (ZKD V) is 1140 ml. For the modern Chinese in our study, the range is between 1110 ml and 1600 ml, with the average volume 1382 ml. Both ZKD V and ZKD X fall within the modern Chinese range. The average volume of the six ZKD endocasts is 1058 ml, which places them in the middle of the range of endocranial volumes obtained for a broad spectrum of *H. erectus* crania ranging from 600 to 1251 ml (Rightmire, 2004). Specimens that may not be *H. erectus* (the Ngandong crania as well as Dmanisi) are included in the calculation. Metric data for fossil endocasts and modern humans are listed in Table 2. All the fossil endocasts are outside the range of the modern Chinese in terms of height and parietal chord.

3.3.2. Non-parametric correlations

Table 3 shows the Spearman rank-order correlations among the dimensions of the ZKD specimens. There are four pairs of correlations that are significant at the 0.01 level: length vs. frontal breadth,

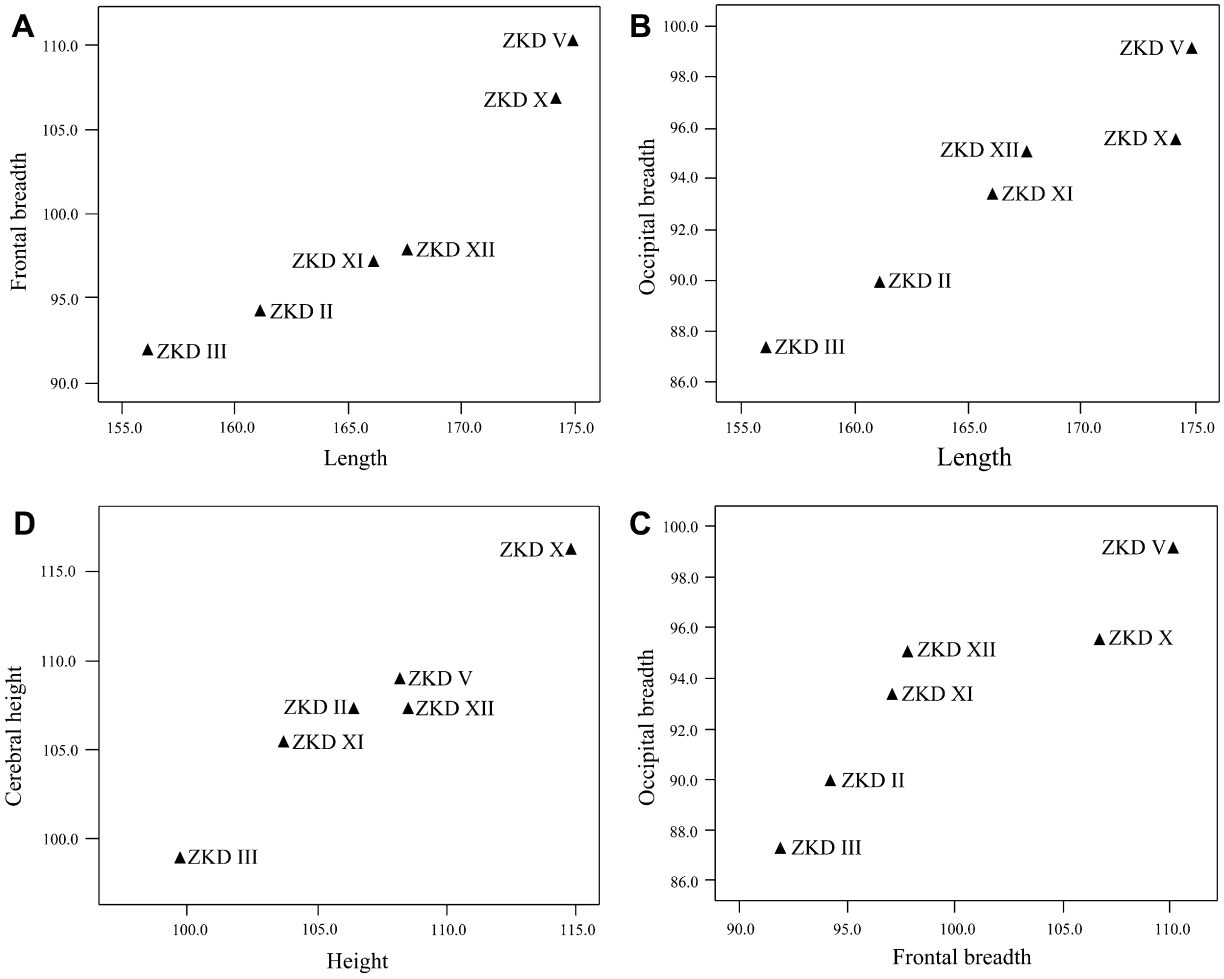

Fig. 4. Bivariate plots of ZKD endocast measures: (A) length vs. frontal breadth, (B) length vs. occipital breadth, (C) height vs. cerebral height, (D) frontal breadth vs. occipital breadth.

Table 4
Principal Components Analysis of nine log measurements of ZKD, other *Homo erectus*, and modern Chinese endocasts.

Variable	Component	
	1	2
Log length	.864	.136
Log breadth	.604	.343
Log height	.942	−.230
Log frontal breadth	.875	−.066
Log cerebral height	.937	−.176
Log frontal height	.918	−.229
Log frontal chord	.584	.242
Log parietal chord	.888	−.162
Log occipital breadth	.443	.742

length vs. occipital breadth, height vs. cerebral height, and frontal breadth vs. occipital breadth.

3.3.3. Bivariate comparisons and non-parametric test

Bivariate plots of selected measures (Fig. 4) illustrate some interesting patterns. In the plots of length vs. frontal breadth (Fig. 4, A), length vs. occipital breadth (Fig. 4, B), and frontal breadth vs. occipital breadth (Fig. 4, D), there are significant relationships between the two increasing measures. ZKD V is wider than the other ZKD specimens in frontal and occipital lobe, and longer than the others in length. Wilcoxon Signed Ranks test shows that length and frontal breadth, length and occipital breadth, and frontal breadth and occipital breadth are significantly different at the 0.01 level ($p = 0.028$). Fig. 4(C) is a plot of height vs. cerebral height at ZKD. ZKD X is higher than the other ZKD specimens. Wilcoxon Signed Ranks test shows that there is no significant difference between height and cerebral height ($p = 0.40$).

3.3.4. Principal component analysis (PCA)

In the PCA of the nine log measures (Table 4 and Fig. 5, A), the first two components account for 74.7% of the total variance. The first component explains 64.6% of the total variation in the data while the second PC explains 10.1%. The highest loadings for PC1 are for three variables that are measures of height: height, cerebral height and frontal height. PC2 has the highest loading for occipital breadth. Fig. 5(A) is a visual representation of the distribution for the endocasts in the subspace of the first two PCs. The modern Chinese cluster together and are principally removed from the fossils (except ZKD X) on PC1. The ZKD specimens are close to Hexian, Trinil II, Sm 3, Sangiran 17, KNM-ER 3733 and Salé on PC1. ZKD II, ZKD III and ZKD XI are close to Trinil II, Sm 3, Sangiran 2, KNM-ER 3733 and Salé on PC2. ZKD X, ZKD XII and ZKD V are close to Hexian, Sangiran 17, Sangiran 12, Sangiran 10, KNM-ER 3883, and KNM-WT 15000 on PC2.

In the PCA of the eight ratio measures (Table 5 and Fig. 5, B), the first two components account for 71.8% of the total variance. The first component explains 48.6% of the total variation in the data while the second PC explains 23.2%. The highest loadings for PC1 are height/length, height/breadth and frontal breadth/breadth. PC2 has the highest loading for occipital breadth/breadth. In Fig. 5(B), the modern Chinese cluster together and are principally removed from the fossils. The ZKD specimens align closely with Hexian, Trinil II, Sm 3, Sangiran 2, Sangiran 12, KNM-ER 3733, Sangiran 17, and Salé. Sangiran 10, KNM-ER 3883 and KNM-WT 15000 are distant from the ZKD specimens.

4. Discussion

The six ZKD *H. erectus* endocasts span over a 300,000 year period, but they have marked morphological similarities. This observation of a general *bauplan*, also emphasized by Weidenreich (1943) for the cranial features, has long been viewed as the defining characteristic of the ZKD sample. Weidenreich did, however, recognize variation among the specimens that he did not attribute to mere sexual dimorphism. Without the benefit of chronometric dating, Weidenreich's ability to appreciate the nature of temporal change at ZKD was limited. He did estimate that ZKD V was possibly the largest of the crania, although later recovery of more fragments did not bear this out (ZKD X is larger). However, ZKD V does exhibit the greatest development of the frontal and occipital breadth expansion documented in this study. Qiu et al. (1973) noted that the ZKD V specimen has more progressive features compared with the other earlier ZKD specimens. Zhang (1991) suggested that there is an evolutionary change in the direction of early *Homo sapiens* morphology in the dental sample from Locality 1. Pei (1985) considered Sinanthropus industry to exhibit certain evolutionary developments, and he divided the Locality 1 industry into three stages: early stage (the artifacts from Layer 11 to Layers 9–8), middle stage (the artifacts from Layers 7 and 6), and late stage (the artifacts from Layers 5–1). The present study supports the idea that the ZKD V specimen is more progressive than the earlier ZKD specimens.

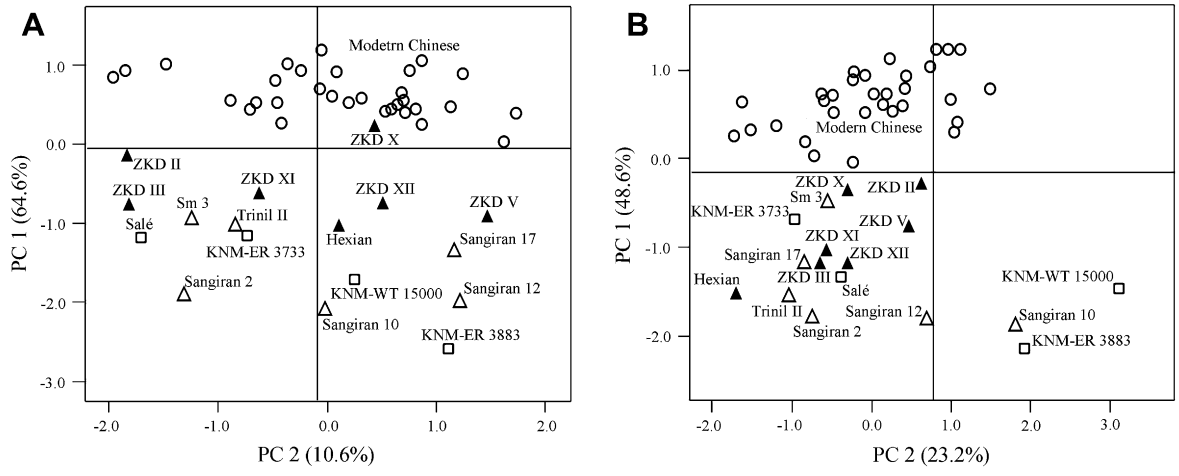

Fig. 5. Principal Components Analysis of ZKD, other fossils and modern Chinese endocasts. (A) Nine variable PCA using log-transformed variables, (B) Eight variable PCA using ratios.

Table 5
Principal Components Analysis of eight ratio measurements of ZKD, other *Homo erectus*, and modern Chinese endocasts.

Variable	Component	
	1	2
breadth/length	−.372	−.729
height/length	.924	.068
height/breadth	.914	.341
occipital breadth/frontal breadth	−.790	.515
frontal chord/parietal chord	−.646	−.029
frontal breadth/breadth	.905	.035
occipital breadth/breadth	−.161	.902
frontal height/cerebral height	.418	−.345

In light of the many new paleoanthropological discoveries over the past 40 years, the taxonomic unity of *H. erectus* has been the subject of much debate. Some researchers propose that the fossil material subsumed under *H. erectus* should be split into African and Asian species (Andrews, 1984; Stringer, 1984; Wood, 1984). Others have argued that no distinct boundary exists between *H. erectus* and *H. sapiens* in time or space, thus, *H. erectus* should be subsumed within the evolutionary species *H. sapiens* (Wolpoff et al., 1994). Some suggest that the ZKD crania possess unique morphological and morphometric features that are not shared by the African and other Asian samples (Kidder, 1998; Anton, 2002, 2003; Kidder and Durband, 2004). Conversely, other researchers argue that cranial features that were regarded as limited to Asian *H. erectus* are also expressed in some African specimens (Braüer, 1994; Rightmire, 1998). Endocast data can be used to address some of these issues.

This study of *H. erectus* endocasts does not document any geographical patterning that could be used to support a separation of the African and Asian specimens. Interestingly, even the six ZKD endocasts from a single locality do not form a discrete cluster with clear separation from the other hominin fossils in our study. Instead, the results document a significant trend for brain expansion over time within *H. erectus*, and basic similarities in the underlying pattern of that expansion where brain enlargement is a function of breadth. This differs from the pattern documented in the modern *H. sapiens*, where height and parietal chord contribute more substantially to changing brain size.

The marked changes in brain shape that occurred over time at ZKD are not clearly evident from simple comparisons of total endocranial volume or linear measurements. ZKD X is a case in point in that it is the largest endocast and plots high above the regression line in the bivariate plots of length vs. frontal breadth, length vs. occipital breadth, and frontal breadth vs. occipital breadth (Fig. 4). The nuances of the temporal changes at ZKD are such that more sophisticated imaging analyses of the separate brain regions' shape and volumes are needed to further evaluate the results of this study and their implications for hominin brain evolution.

5. Conclusions

Documentation of the overwhelming morphological similarity of the six ZKD endocasts, that are known to represent a 300,000 year time span, has significant relevance for our understanding of *H. erectus* and hominin evolution and highlights the importance of detailed site-specific analyses. The ZKD brain casts share several features (low height and low position of the greatest breadth, flat frontal and parietal lobes, depressed Sylvian areas, strong posterior projection of the occipital lobes, anterior positioning of the cerebellar lobes relative to the occipital lobes, and relative simplicity of the meningeal vessels) that distinguish them from the modern Chinese. All of the fossils are outside the range of the modern Chinese; they are characterized by much lower height measurements and have low height dimensions and shorter parietal chord. It is this aspect, more than any other feature, which can be regarded as the definitive characteristic of presapiens members of the genus *Homo*.

Despite their general similarities, the ZKD endocasts also provide evidence for significant changes in components of brain breadth that are correlated with geologic time. The youngest fossil in the sequence, ZKD V, has the greatest expansion of the frontal and occipital lobes. In this capacity it exceeds ZKD X, the cranium with the largest volume. For these reasons, it is important to factor the temporal variation of the ZKD hominin fossils into considerations of *H. erectus* evolution.

Acknowledgments

We are grateful to Yinyun Zhang for his help in preparing the endocast of ZKD V and his useful suggestions and encouragement. This project is supported by the Knowledge Innovation Program of the Chinese Academy of Sciences (Grant No: KZCX2-YW-106), the International Cooperation Program of MST of China (Grant No: 2007DFB20330), the National Science Fund of China (Grant No: 40772018) and the State Key Laboratory of Palaeobiology and Stratigraphy of Nanjing Institute of Geology and Palaeontology (Grant No: 093109).

References

Andrews, P., 1984. An alternative interpretation of the characters used to define *Homo erectus*. Courier Forshungsinstitut Senckenberg 69, 167–175.
Anton, S., 2002. Evolutionary significance of cranial variation in Asian *Homo erectus*. American Journal of Physical Anthropology 118, 301–323.
Anton, S., 2003. Natural history of *Homo erectus*. Yearbook of Physical Anthropology 46, 126–170.
Ariens-Kappers, C.U., 1934. The fissuration on the frontal lobe of *Sinanthropus pekinensis* Black, compared with the fissuration in Neanderthal men. Proceedings of the Koninklijke Nederlandse Akademie van Wetenschappen 36, 802–812.
Ariens-Kappers, C.U., Bouman, K.H., 1939. Comparison of the endocranial casts of the *Pithecanthropus erectus* skull found by Dubois and von Koenigswald's *Pithecanthropus* skull. Proceedings of the Koninklijke Nederlandse Akademie van Wetenschappen 42, 30–40.
Begun, D., Walker, A., 1993. The endocast. In: Walker, A., Leakey, R. (Eds.), The Nariokotome *Homo erectus* Skeleton. Harvard University Press, Cambridge, pp. 326–358.
Black, D., 1932. The brain cast of *Sinanthropus*, a review. Journal of Comparative Neurology 56, 361–366.
Black, D., 1933. On the endocranial cast of the adolescent *Sinanthropus* skull. Proceedings of the Royal Society B 112, 263–276.
Black, D., de Chardin, T., Young, C.C., Pei, W.C., 1933. Fossil man in China. The Geological Survey of China and The Section of Geology of the National Academy of Peiping. Peiping 11, 1–166.
Braüer, G., 1994. How different are Asian and African *Homo erectus*? Courier Forshungsinstitut Senckenberg 171, 301–318.
Broadfield, D.C., Holloway, R.L., Mowbray, K., Mowbray, K., Silvers, A., Yuan, M.S., Márquez, S., 2001. Endocast of Sambungmacan 3 (Sm 3): a new *Homo erectus* from Indonesia. Anatomical Record 262, 369–379.
Brown, F.H., McDougall, I., 1993. Geologic setting and age. In: Walker, A., Leakey, R. (Eds.), The Nariokotome *Homo erectus* Skeleton. Harvard University Press, Cambridge, pp. 9–20.
Brown, F.H., Harris, J., Leakey, R., Walker, A., 1985. Early *Homo erectus* skeleton from west Lake Turkana, Kenya. Nature 316, 788–792.
Bruner, E., 2003. Fossil traces of the human thought: paleoneurology and the evolution of the genus *Homo*. Rivista di Antropologia 81, 29–56.
Bruner, E., 2004. Geometric morphometrics and paleoneurology: brain shape evolution in the genus *Homo*. Journal of Human Evolution 47, 279–303.
Delson, E., Harvati, K., Reddy, D., Marcus, L.F., Mowbray, K., Sawyer, G.J., Jacob, T., Márquez, S., 2001. The Sambungmacan 3 *Homo erectus* calvaria: a comparative morphometric and morphological analysis. Anatomical Record 262, 380–397.
Dubois, E., 1933. The shape and size of the brain in *Sinanthropus* and in *Pithecanthropus*. Proceedings Royal Academy of Amsterdam 36, 1–9.
Falk, D., 1985. Hadar AL162-28 endocast as evidence that brain enlargement preceded cortical reorganization in hominid evolution. Nature 313, 45–47.
Grimaud-Hervé, D., 1997. L'évolution de l'enchéphale chez *Homo erectus* et *Homo sapiens*. CNRS Editions, Paris, pp. 1–420.

Grün, R., Huang, P.H., Wu, X.Z., Stringer, C.B., Thorne, A.G., McCulloch, M., 1997. ESR analysis of teeth from the palaeoanthropological site of Zhoukoudian, China. Journal of Human Evolution 32, 83–91.
Grün, R., Huang, P.H., Huang, W.P., McDermott, F., Thorne, A., Stringer, C.B., Yan, G., 1998. ESR and U-series analyses of teeth from the palaeoanthropological site of Hexian, Anhui Province, China. Journal of Human Evolution 34, 555–564.
Holloway, R.L., 1980. Indonesian "Solo" (Ngandong) endocranial reconstructions: some preliminary observations with Neanderthal and *Homo erectus* groups. American Journal of Physical Anthropology 53, 285–295.
Holloway, R.L., 1981. The Indonesian *Homo erectus* brain endocasts revisited. American Journal of Physical Anthropology 55, 503–521.
Holloway, R.L., De La Coste-Lareyondie, M.C., 1982. Brain endocast asymmetry in pongids and hominids: some preliminary findings on the paleontology of cerebral dominance. American Journal of Physical Anthropology 58, 101–110.
Holloway, R.L., Broadfield, D.C., Yuan, M.S., 2004. The Human Fossil Record. In: Brain Endocasts—the Paleoneurological Evidence, vol. 3. Wiley-Liss, New York.
Huang, P.H., Jin, S.Z., Peng, Z.C., Liang, R.Y., Lu, Z.J., Wang, Z.R., Chen, J.B., Yuan, Z.X., 1993. ESR dating of tooth enamel: comparison with U-Series, FT and TL dating at the Peking Man Site. Applied Radiation and Isotopes 44, 239–242.
Jia, L.P., 1959. Report on the excavation of *Sinanthropus* site in 1958. Vertebrate Palaeontology 1, 21–26.
Kidder, J.H., 1998. Morphometric variability in *Homo erectus*. American Journal of Physical Anthropology 24 (Suppl.), 138.
Kidder, J.H., Durband, A.C., 2004. A re-evaluation of the metric diversity within Homo erectus. Journal of Human Evolution 46, 297–313.
LeMay, M., Billing, M.S., Geschwind, N., 1982. Asymmetries of the brains and skulls. In: Armstrong, E., Falk, D. (Eds.), Primate Brain Evolution. Plenum Press, New York, pp. 263–277.
Lin, S.L., 2004. The first skull of Peking man was found in layer 11, not in layer 10. Acta Anthropology Sinica 23, 173–186.
Pei, J.X., 1985. Thermoluminescence dating of the Peking Man site and another cave. In: Wu, R.K., Ren, M.E., Zhu, X.M., Yang, Z.G., Hu, C.K., Kong, Z.C., Xie, Y.Y., Zhao, S.S. (Eds.), Multi-disciplinary Study of the Peking Man Site at Zhoukoudian. Science Press, Beijing, pp. 256–260 (in Chinese).
Pei, W.C., 1929. An account of the discovery of an adult *Sinanthropus* skull in the Choukoutien deposit. Bulletin of the Geological Society of China 8, 203–250.
Qiu, Z.L., Gu, Y.M., Zhang, Y.Y., Zhang, S.S., 1973. Newly discovered *Sinanthropus* remains and stone artifacts at Zhoukoudian. Vertebrata Palasiatica 11, 109–131.
Rightmire, G.P., 1998. Evidence from facial morphology for similarity of Asian and African representatives of *Homo erectus*. American Journal of Physical Anthropology 106, 61–85.
Rightmire, G.P., 2004. Brain size and encephalization in early to mid-Pleistocene *Homo*. American Journal of Physical Anthropology 124, 109–123.
Shellshear, J.L., Smith, G.E., 1934. A comparative study of the endocranial cast of *Sinanthropus*. Philosophical Transactions of the Royal Society of London Series B 223, 469–487.
Shen, G., Ku, T., Cheng, H., Edwards, R., Yuan, Z., Wang, Q., 2001. High-precision U-series dating of Locality 1 at Zhoukoudian, China. Journal of Human Evolution 41, 679–688.
Shen, G., Gao, X., Gao, B., Granger, D., 2009. Age of Zhoukoudian *Homo erectus* determined with $^{26}Al/^{10}Be$ burial dating. Nature 458, 198–200.
Stringer, C., 1984. The definition of *Homo erectus* and the existence of the species in Africa and Europe. Courier Forshungsinstitut Senckenberg 69, 131–143.
Swisher III, C.C., Curtis, G.H., Jacob, J., Getty, A.G., Suprijo, A., Widiasmoro, 1994. Age of the earliest known hominids in Java, Indonesia. Science 263, 1118–1121.
Weidenreich, F., 1935. The *Sinanthropus* population of Choukoutien (Locality 1) with a preliminary report on new discoveries. Bulletin of the Geological Society of China 14, 427–461.
Weidenreich, F., 1936. Observations on the form and proportions of the endocranial casts of *Sinanthropus pekinensis*, other hominids and the great apes: a comparative study of brain size. Paleontologica Sinica NSD 7, 1–50.
Weidenreich, F., 1938. The ramification of the middle meningeal artery in fossil hominids and its bearing upon phylogenetic problems. Paleontologica Sinica, New Series D 3, 1–16.
Weidenreich, F., 1941. The brain and its role in the phylogenetic transformation of the human skull. Transactions of the American Philosophical Society, New Series 31, 321–442.
Weidenreich, F., 1943. The skull of *Sinanthropus pekinensis*: a comparative study on a primitive hominid skull. Paleontologica Sinica, New Series 10, 108–113.
Wood, B.A., 1984. The origin of *Homo erectus*. Courier Forshungsinstitut Senckenberg 69, 99–111.
Wolpoff, M.H., Thorne, A.G., Jelínek, J., Zhang, Y.Y., 1994. The case for Sinking *Homo erectus*. 100 Years of *Pithecanthropus* is Enough!. Courier Forschungsinstitut Senckenberg 171, 341–361.
Wu, R.K., Dong, X.R., 1982. Preliminary study of *Homo erectus* remains from Hexian, Anhui. Acta Anthropologica Sinica 1, 2–13.
Wu, X.J., Schepartz, L., Falk, D., Liu, W., 2006. Endocast of Hexian *Homo erectus* from south China. American Journal of Physical Anthropology 130, 445–454.
Wu, X.J., Schepartz, L., Liu, W., 2009. Endocranial cast of Zhoukoudian skull V: a new *Homo erectus* brain endocast from China. Proceedings of the Royal Society B. doi:10.1098/rspb.2009.0149 Published online before print April 29, 2009.
Zhang, Y.Y., 1991. An examination of temporal variation in the hominid dental sample from Zhoukoudian Locality 1. Acta Anthropologica Sinica 10, 85–95.